Integrating multiple spheres to identify the provenance and risk of urban dust and potentially toxic elements: Case study from central Mexico

Original Submission

submitted to:

Environmental Pollution

Integrating Multiple Spheres to Identify the Provenance and Risk of Urban Dust and Potentially Toxic Elements: Case Study from Central Mexico

Rodrigo Rodríguez[a], Diana Meza-Figueroa[b], Agustin Robles-Morua[c], José Tuxpan-Vargas[a], Elena Vázquez-Vázquez[d], Bhaskar Sen-Gupta[e] and Nadia Martínez-Villegas[a,*]

[a]IPICYT, Instituto Potosino de Investigación Cientifica y Tecnologica, Division de Geociencias Aplicadas, Camino a la Presa San Jose No. 2055, Col. Lomas 4a Sec., C.P. 78216, San Luis Potosi, SLP, Mexico.
[b]UNISON, Universidad de Sonora, Departamento de Geología, Rosales y Encinas s/n, C.P. 83000, Hermosillo, Sonora, Mexico.
[c]ITSON, Instituto Tecnológico de Sonora, Departamento de Ciencias del Agua y del Medio Ambiente, 5 de febrero No. 818 sur, Col. Centro, C.P.85000, Cd. Obregón, Sonora, Mexico.
[d]UASLP, Universidad Autónoma de San Luis Potosí, Instituto de Metalurgia, Sierra Leona No. 550, Col. Lomas 2a Sec, C.P. 78210, San Luis Potosi, SLP, Mexico.
[e]Heriot Watt University, School of Energy, Geoscience, Infrastructure and Society, Room 2.02A, William Arrol Building, EH14 4AS, Heriot Watt University, Edinburgh, United Kingdom.

*Corresponding author
Nadia Martínez-Villegas
Camino a la Presa San Jose No. 2055
Lomas 4a Sec
San Luis Potosi, SLP 78216
Mexico.
e-mail: nadia.martinez@ipicyt.edu.mx
Phone: +52(444)834-2000 x-7272
Fax: 52 (444)834-2010

Abstract

This study aims to improve the current method of studying potentially toxic elements (PTEs) in urban dust using direct chemical evidence (from dust, rock, and emission source samples) and robust geochemical methods. The provenance of urban dust was determined using REEs and geochemical diagrams (V-Ni-Th*10, Zr vs. TiO2, and Zr/Ti vs. Nb/Y). The geogenic or anthropogenic source of PTEs was determined using the enrichment factor (EF) and compositional data analysis (CoDA), while PTE's point emission source was identified using a 3.1*La-1.54*Ce-Zn diagram, mineralogy, and morphology analyses. The spatiotemporal distribution of PTEs was determined using a geographic information system, and their health risk (by inhalation) was estimated using a lung bioaccessibility test and particle size distribution. We collected urban dust (n=38), rock (n=4), and zinc concentrate (n=2) samples and determined PTEs and rare earth elements (REEs) in a city of 1.25 million inhabitants in central Mexico. Results showed that urban dust derived from the San Miguelito Range. REEs, Sc, and Zr were geogenic, while Mn, Cu, Zn, As, and Pb were anthropogenic. Due to sphalerite particle dispersion, a zinc refinery (ZR) was identified as the point emission source of Zn, As, and Pb. High concentrations of Zn (5000-20,008 mg/kg), As (120-284 mg/kg), and Pb (350-776 mg/kg) were found in urban dust near the ZR. Additionally, particles of PM2.5 (66-84%), PM5.0 (13-27%), PM10 (3-8%), and PM20 (0-2%) and lung bioaccessibility of Sr (48.5-72.4%), Zn (9.6-28.4%), Cu (10.5-27.0%), Fe (4.5-8.6%), Mn (2.9-9.2%), Cr (38.3%) and Pb (30.6%) demonstrated a latent risk to human health. These approaches improve our understanding of the provenance of urban dust and its PTE emissions sources in urban areas.

keywords: urban dust, potentially toxic elements, geochemistry analysis, emission sources, health risk assessment.

1. Introduction

Urban dust are heterogeneous particles deposited on the urban surface and an important sink for potentially toxic elements (PTEs) (Teran et al., 2020). These particles can come from various sources, including geological settings, soil, pollen, and even anthropogenic sources such as vehicle exhaust, construction sites, and industrial emissions. High concentrations of PTEs (such as Pb, As, Zn, Cu, Cr, and V) have been reported in urban dust all over the world, mainly in industrial or mining cities (Fan et al., 2022; Lima et al., 2023; Meza-Figueroa et al., 2018). Urban dust particles <10 μm are highly hazardous due to their ability to enter the respiratory system by inhalation (Plumlee & Ziegler, 2007), where PTEs may dissolve in lung fluids, causing systemic toxicity (Innes et al., 2021), and represent a risk to human health. Dust of geogenic provenance has been documented to be affected by anthropogenic activities, such as traffic and industry, and appears to be an important means of transport of PTEs in urban environments (Moreno-Rodríguez et al., 2015). In addition, dust particles can transport PTEs over long distances, affecting their transport, fate, and concentrations in urban environments. Humans can be exposed via ingestion, inhalation, and dermal contact (Meza-Figueroa et al., 2018). Therefore, it is urgent to accurately identify the origin of urban dust and the geogenic and/or anthropogenic sources of PTEs.

However, the study of the provenance of urban dust is limited (Dehghani et al., 2018). Most studies have taken approaches focused only on the elemental characterization of PTEs in urban dust and adopted statistical and documentary methods to differentiate, at most, the geogenic or anthropogenic origin of PTEs in urban dust (Bourliva et al., 2018; Fan et al., 2022; Gaberšek et al., 2022; Fan et al., 2022; Lima et al., 2023; Teran et al., 2020), leaving out strong chemical evidence on the provenance of urban dust and PTEs. Attempts have been made to trace the emission sources of PTEs that contaminate dust. For example, using the Positive Matrix

Factorization (PMF) model is possible to determine the contribution of natural sources, mixed sources (industrial activities and transport), or agricultural sources to the content of PTEs in urban dust (Haung et al., 2022; Huang et al., 2022, 2023). Like other multivariate statistical analyses, PMF only identifies groups of sources but not specific point sources.

The novelty of the present investigation is to expand sampling plans to geological and likely contamination sources and use chemical tools to determine urban dust and PTEs origin and sources accurately. For example, the use of rare earth elements (REEs), resistant to environmental conditions (Moreno et al., 2006), might provide urban dust chemical fingerprint to trace its origin. REEs have been used to determine the provenance of sediments and soils (González-Guzmán et al., 2022; Huyan & Yao, 2022) as they do not fractionate easily during sedimentation and weathering (Dehghani et al., 2018; González-Guzmán et al., 2022; Moreno et al., 2006). In addition, the use of immobile trace elements (Ti, Al, Zr, Hf, Th, Nb, Y) has been used to trace the genetic relationship between soils or sediments and their parent material/lithology (Arruda et al., 2023; Wei et al., 2023). The classical diagrams of Ni-V-Th*10 (Bracciali et al., 2007), TiO_2-Zr (Hayashi et al., 1997), and Zr/Ti vs. Nb/Y (Pearce, 1996), using immobile trace elements, might help trace the genetic relationship between urban dust and its parent material, as well as its geochemical classification. Furthermore, the use of concentrations of trace elements might help identify emission sources of PTEs. For example, Ni and V have been used to identify refinery emissions as specific point emission sources of PTE in soils and atmospheric particles (González-Guzmán et al., 2022; Moreno et al., 2008, 2010). However, these methodologies have never been applied to PTEs in urban dust. In contrast, mineralogy and particle morphology have been used to identify specific PTE sources in urban dust (Meza-Figueroa et al., 2018; Trechera et al., 2020). More comprehensive sampling approaches and the incorporation of adjacent chemical

methodologies currently used in the study of sediments, soils, and atmospheric particles will help to better understand the provenance of urban dust and PTEs spatially and seasonally in urban settings, especially in arid and semi-arid areas, where urban dust is common ground and might represent health risk (Choobari et al., 2014).

With this in mind, our hypothesis is that the integration of urban dust, geological, and pollution source samples, along with sound chemical analysis, accurately identifies the geogenic and anthropogenic sources of PTE in urban dust. The objectives of this study were to determine: i) the urban dust provenance using REEs concentrations and geochemical diagrams (V-Ni-Th*10, Zr vs. TiO_2, and Zr/Ti vs. Nb/Y), ii) the geogenic or anthropogenic origin of PTEs in urban dust using PTE concentrations, the enrichment factor (EF), and compositional data (CoDA), iii) the potential emission sources of PTEs using a modified version of the 3.1*La-1.54*Ce-V geochemical diagram and urban dust mineralogy, elemental composition, and morphology, iv) the spatial and seasonal distribution of PTEs using PTE concentrations and a geographical information system, and v) the health risk posed by PTEs by measuring particle size and determining lung bioaccessibility. The results of this study will help improve the comprehension of environmental issues in urban systems which are of global interest given that more than 55% of the world population currently lives in urban areas and this is expected to increase to 68% by 2050 (UN, 2019).

2. Methodology

2.1. Study area

This study was carried out in the San Luis Potosi Metropolitan Area (SLPMA), which includes the municipalities of San Luis Potosi and Soledad de Graciano Sanchez in central Mexico

123 (Figure 1), and which accounts for 1,243,980 people, settled in an area of 1,787.7 km^2 (INEGI,
124 2021). The SLPMA basin was selected as our study area because it is filled with alluvial sediments
125 and polymictic conglomerates, and surrounded, to the south, by the volcanic complex of the San
126 Miguelito Mountain Range, comprising of ignimbrites, ignimbrite-rhyolite tuff, rhyolite, and
127 andesites (Figure 1) (SGM, 1998). In addition, the SLPMA has a zinc refinery (ZR) that processes
128 easily dispersible zinc concentrates from the Santa Bárbara and Charcas mines found on the west
129 of the SLPMA (Figure 1). Additionally, a copper and an arsenic plant that operated from 1925
130 through to 2010 are located next to the ZR (Martínez Jardines, 2018). High concentrations of Zn,
131 Pb, As, and Cu were reported in soils and atmospheric particles (Carrizales et al., 2006; Piña et al.,
132 2002) near the ZR as well as in the urine and blood of children living around the ZR and the copper
133 and arsenic plants (Carrizales et al., 2006). Also, the presence of Zn, Cu, and Pb in urban dust was
134 attributed to the ZR (Aguilera et al., 2019). The largest industrial area of the SLPMA is found to
135 the south-southeast (Figure 1), where automotive, foundry, metalworking, and hazardous waste
136 management industries operate, among others (Ortega Montoya et al., 2014).
137 The SLPMA's climate is semi-arid (González Medrano, 2012) with short but high-intensity
138 precipitation events that often result in flooding of the urban area (Barboza Gudiño, 2018), which
139 has been subdivided into 12 urban basins (Figure 1) (Rodríguez Rodríguez, 2020). Predominant
140 wind direction is towards the east, north, and southwest before the rainy season, while predominant
141 wind moves mainly towards the east after the rainy season (CONAGUA, 2019). The average
142 annual precipitation is 407 mm (CONAGUA, 2018). The rainy season occurs from May to October
143 with an average precipitation of 46 mm, while the dry season occurs from November to April with
144 an average precipitation of 12 mm (CONAGUA, 2018).

Figure 1. Geographical location of SLPMA showing the lithology, the urban basins, and the sampling points for urban dust, rocks, and zinc concentrate analyses.

2.2. Sampling urban dust, rocks, and zinc concentrates

Urban dust samples were collected from paved streets, and distributed in the upper, middle, and lower topographical latitudes of U2, U3, U4, U5, U6, U7, U8, and U9 urban basins (Figure 1). Sample collection was carried out twice in 2019 to capture seasonal variations. The first sampling campaign was carried out in March, before the rainy season, using brushes and polyethylene collectors, while the second sampling campaign was in November, after the rainy

154 season (Meza-Figueroa et al., 2007). Urban dust samples were oven-dried at 40°C for 24 h. Rock
155 samples were collected from ignimbrite, rhyolite, ignimbrite-rhyolitic tuff, and andesite
156 lithological compositions in the study area (Figure 1). One rock sample, representative of each
157 lithological unit (Aguillón-Robles et al., 2012, 2014; Torres-Sánchez et al., 2019, 2020), was
158 collected according to reports found in the literature to trace the provenance of heavy metals in
159 soils (González-Guzmán et al., 2022). Rock samples were crushed and pulverized using a Fritsch
160 Planetary Mono Mill Pulverisette agate mill. Zinc concentrate samples were obtained from the
161 Santa Bárbara and Charcas mines. All urban dust, rock, and zinc concentrate samples were sieved
162 at <20 μm using a SS-30 Ro-Tap device and stored in polypropylene bags until further analysis.

163 ### *2.3. Determining urban dust provenance*

164 Urban dust (n=10), rock (n=4), and zinc concentrate (n=2) samples were analyzed to
165 determine REE (La, Ce, Pr, Nd, Sm, Eu, Gd, Tb, Dy, Ho, Er, Tm, Yb, and Lu) and Th, Ni, V, Ti,
166 Zr, Nb, and Y concentrations. REEs and Th, Ni, V, Ti, Zr, Nb, and Y concentrations were
167 determined in triplicates in 0.1 g of sample digested with 10 mL of HF (49%), 30 mL of HCl
168 (36%), and 10 mL of HNO3 (65%). Digestions were carried out in Teflon vessels at 180 °C for
169 approximately 6 h until the samples completely dissolved and the acids evaporated. The resulting
170 salts were dissolved in 2% HNO_3 and transferred to a 25 mL flask to make up to volume. For
171 quality assurance and control, the Montana Soil NIST 2710a and ^{103}Rh reference standards and
172 five blanks were used. Elemental concentrations were determined using inductively coupled
173 plasma mass spectrometry (ICP-MS) in a ThermoScientificTM iCAPTM-RQ instrument, in
174 Kinetic Energy Discrimination (KED) mode, according to Method 6020B (EPA, 2014). REE
175 concentrations were normalized to the upper continental crust (UCC) (Taylor & McLennan, 1985)
176 to determine the provenance of urban dust by comparison of urban dust fingerprinting to rock and

zinc concentrate fingerprinting. The Ni-V-Th*10 (Bracciali et al., 2007), TiO_2-Zr (Hayashi et al., 1997), and Zr/Ti vs. Nb/Y (Pearce, 1996) diagrams were used to trace the felsic, mafic, or ultramafic provenance of urban dust and its geochemical classification.

2.4. Determining geogenic or anthropogenic origin of PTE

The enrichment factor (EF) was used to determine the anthropogenic impact of the SLPMA on urban dust using average elemental concentrations of local rocks and aluminum (Al) as background and normalization values, respectively, using Equation 1 (Zoller et al., 1974):

(Equation 1) $$EF_i = \frac{C_{i,dust}/Al_{dust}}{C_{i,rock}/Al_{rock}}$$

Where EF_i was the enrichment factor of the i^{th} PTE, $C_{i,dust}$ was the concentration of the i^{th} PTE in the dust (mg/kg), Al_{dust} was the concentration of normalization element (Al) in the dust (mg/kg), $C_{i,rock}$ was the concentration of the i^{th} PTE in the rock (mg/kg), and Al_{rock} was the concentration of normalization element (Al) in the rock (mg/kg). Aluminum and PTE (Fe, Zn, Mn, Cu, Pb, Sc, Sr, Zr, Cr, As, and V) concentrations were determined during REE analyses. The use of EF was preferred over the pollution index (PI) or the geoaccumulation index (Igeo) due to its normalization using a weathering-resistant element, such as Al (Bern et al., 2019), Aluminum is a relatively stable and abundant element in the Earth's crust, making it a suitable reference for normalization (Ho et al., 2012; Merli et al., 2020). Additionally, Al is commonly used as a reference element in geochemical studies because its concentrations are less likely to be influenced by anthropogenic activities (Ho et al., 2012; Ma et al., 2016; Pereira et al., 2019; Sappa et al., 2020). Furthermore, Al exhibited relatively uniform concentrations in our rock and urban dust samples and displayed a statistically significant positive correlation with REEs (Table S5, Supplementary Material).

Compositional data analysis (CoDA) was used to transform geochemical data in this study (Text S1, Supplementary Material). REE and PTE concentrations from urban dust, rock, and zinc concentrate samples were transformed using the center log ratio (clr) transformation. Afterwards, principal components analysis (PCA), multivariate statistical analysis, and clustering were carried out. The functions pcaCoDa, corCoDa, and clustCoDa from the "compositions" library were used (Van den Boogaart et al., 2022). The criterion for selecting the number of components in PCA analyses was an eigenvalue > 1. Any variables with a load ≥ 0.3 were considered to impact contribution to the component, while any variables with a load ≤ -0.3 were considered to contribute negatively the component (Wheeler et al., 2021). Since the CoDa correlations do not generate p-values, the "psych" library and the Pearson correlation method on transformed data were used to estimate significant correlations ($p<0.05$) (Revelle, 2021).

2.5. Determining the sources of PTE

A 3.1*La-1.54*Ce-V modified ternary diagram (i.e., 3.1*La-1.54*Ce-Zn) was used to identify the source of PTEs in urban dust. The 3.1*La-1.54*Ce-V ternary diagram (using V) is commonly used to compare geochemical signatures between soils or atmospheric particles and potential emission sources (such as Earth's crust, refineries, power plants, and industrial districts) (Moreno et al., 2008). However, in this study, a modified version of the 3.1*La-1.54*Ce-V diagram, substituting V for Zn was used (i.e., 3.1*La-1.54*Ce-Zn), as the ZR in SLPMA seemed to impact urban dust (Figure S2, Supplementary Material). Additionally, the zinc concentrate mineralogy was determined by X-ray powder diffraction (XRD) using a SmartLab RIGAKU X-ray diffractometer over a 2-theta range of 5° to 90°. Mineral phase identification was carried out using the crystallography open database (COD-Inorg Rev.210714), updated in July 2021, and the MATCH3 (Phase Identification from Powder Diffraction) v3.8 program for Windows. The semi-

quantitative determination of the mineral phases was carried out using MATCH3. The elemental composition and morphology of the zinc concentrate was investigated using Scanning Electron Microscopy (SEM) coupled with Energy-dispersive X-ray spectroscopy (EDS) as well as by using a Thermo Fisher Scientific Phenom Pro Scanning Electron Microscope.

2.6. Determining the spatial and seasonal distribution of PTE

The spatiotemporal distribution of Fe, Zn, Mn, Cu, Pb, Sc, Sr, Zr, Cr, As, and V in urban dust, pre and post rainy season, were mapped using ArcGIS 10.3 and the inverse distance weighting (IDW) interpolation method. To do so, a total of 38 urban dust samples (<20μm) (Figure 1) were analyzed by X-ray fluorescence (XRF) using a ThermoScientific Niton FXL X-ray fluorescence device to determine elemental concentrations following the 6200 method (USEPA, 2007). All samples were run in triplicates for 60 seconds using silicon dioxide (SiO_2) as a blank. Average recoveries for all elements were acceptable (between 98 and 114%), according to the 80 to 120% acceptable range (USEPA, 2007). Detection limits for Fe, Zn, Mn, Cu, Pb, Sc, Sr, Zr, Cr, As, and V in silicon dioxide (SiO_2) were 16, 3, 24, 6, 2, 2, 1, 1, 5, 2, and 4 mg/kg, respectively. The Montana Soil NIST 2710a was used for quality control.

2.7. Determining health risk

A total of 8 urban dust samples (with the highest concentrations of PTEs per urban basin), pre and post rainy season, were used to determine urban dust particle size distribution and PTE lung bioaccessibility (Figure 1). Particle size distributions were determined by introducing urban dust into a particle resuspension chamber where urban dust was resuspended (using air), further deposited in a sample holder (by gravity) (Meza-Figueroa et al., 2020), and analyzed using a Thermo Fisher Scientific Phenom Pro scanning electron microscope and the Phenom ParticleMetric software. Lung bioaccessibility was determined in duplicates in 0.01 g of urban

dust <20 μm digested with 10 ml of artificial lysosomal fluid (ALF). Digests were carried out in Teflon vessels at a 1:1000 (w:v) ratio, pH 4.5, and 37°C in an incubator for 24 h with an orbital shaker (Table S1, Supplementary Material) (Colombo et al., 2008; Meza-Figueroa et al., 2020). All digests were filtered (0.2 μm) and frozen until further analysis by inductively coupled plasma optical emission spectroscopy (ICP-OES) using a Varian 730 ES spectrometer. The percentage of lung bioaccessibility was calculated using Equation 2 (Guney et al., 2017):

(Equation 2) $$Bio_i = \frac{C_{i,ALF}\,V}{C_{i,total}\,m} \times 100[=]\%$$

Where Bio_i was the lung bioaccessibility of the i^{th} PTE, $C_{i,ALF}$ was the concentration of the i^{th} PTE in the ALF solution (mg/L), V was the volume of the ALF solution (L), $C_{i,total}$ was the concentration of the i^{th} PTE in the urban dust sample (mg/kg), and m was the mass of the sample (kg). For quality assurance and control, two ALF blanks and the NIST 2710a reference material were used to compare the results obtained in this study and others (Kastury et al., 2018; Meza-Figueroa et al., 2020; Pelfrêne et al., 2017), using Equation 3:

(Equation 3) $$R_{Bioi,NIST} = \frac{Bio_{i,NIST,this\ study}}{Bio_{i,NIST,another\ study}} \times 100[=]\%$$

Where $R_{Bioi,NIST}$ was the recovery of the bioaccessibility of the i^{th} PTE extracted from the NIST reference material (%), $Bio_{i,NIST,\ this\ study}$ was the bioaccessibility of the i^{th} PTE extracted from the NIST reference material in this study (%), $Bio_{i,NIST,\ another\ study}$ was the bioaccessibility of the i^{th} PTE extracted from the NIST reference material in another study (%), assuming that the latter was that stated by bioaccessibility of the i^{th} PTE in the NIST reference material and that both experiments were carried out under the same conditions. Recoveries close to 100% suggested a good analytical precision or exactitude.

To determine statistically significant differences for i) PTE concentrations, ii) particle sizes, and iii) lung bioaccessibility between pre and post rainy season sampling, one-way analysis of variance (ANOVA) and robust generalization methods were used with the Welch and Box with the functions t1way and box1way (p-value = 0.05), respectively, from the "WRS2" library. Equal variances (homoscedasticity) and normality of the data were not assumed, p-values ≤ 0.05 were considered significantly different (Mair & Wilcox, 2020; Wilcox, 2011). All statistical analyses were carried out in R 4.3.0 (R Core Team, 2023).

3. Results and discussion

3.1. The provenance of urban dust

Figure 2a shows the normalized fingerprinting patterns of REEs to UCC in rock, urban dust, and zinc concentrate samples, revealing higher $REE_{samples}/REE_{UCC}$ ratios in rock and urban dust samples than in zinc concentrates. Additionally, a negative Eu anomaly was observed only between rocks and urban dust (Figure 2a), suggesting that urban dust in the SLPMA derived from local rocks from the San Miguelito Mountain Range. Eu anomalies might derive from the fractionation of plagioclase minerals from the volcanic complex of the San Miguelito Mountain Range during partial melting of magmas (Torres-Sánchez et al., 2019).

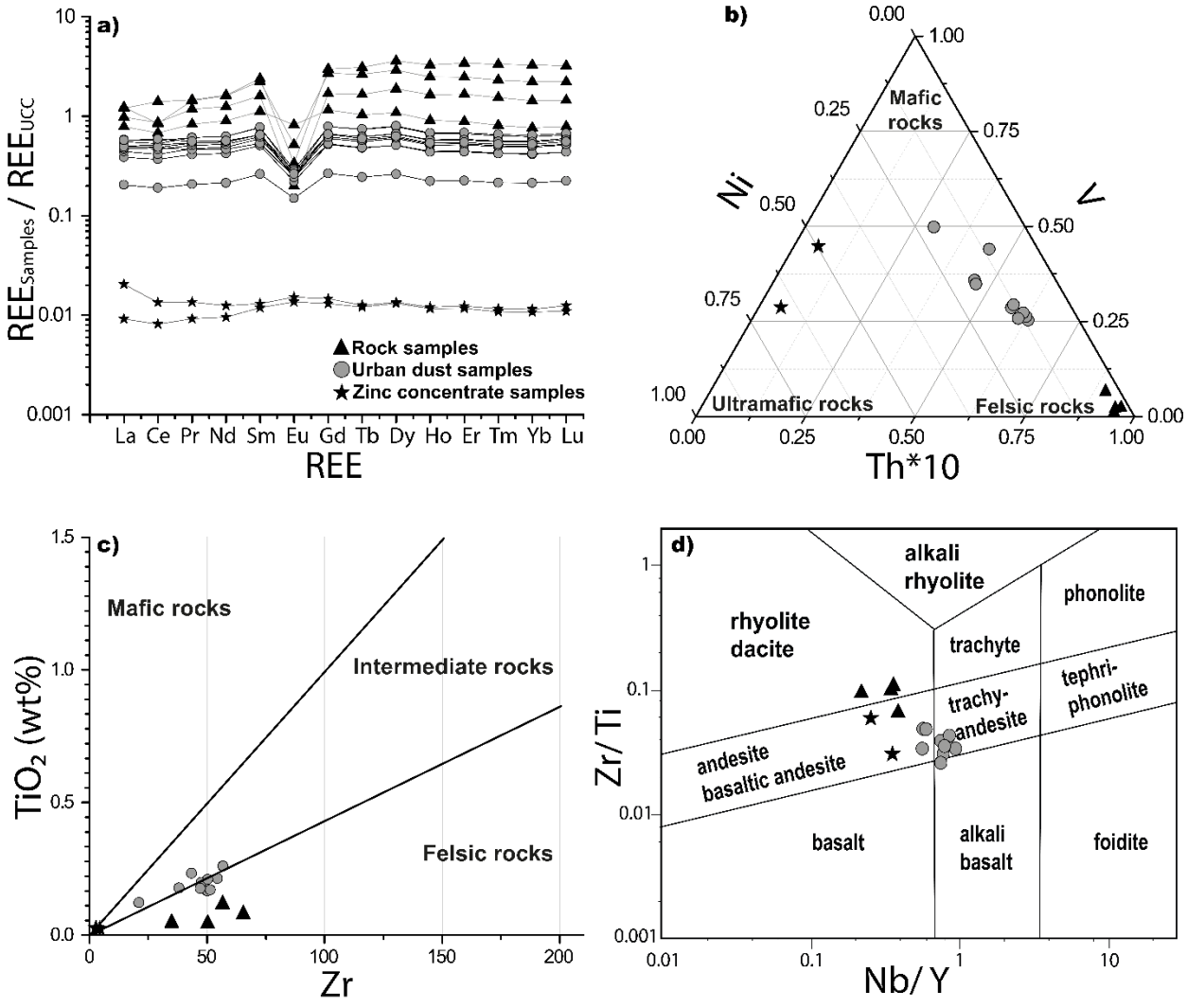

Figure 2. a) REE concentrations normalized to UCC in rock, urban dust, and Zn concentrate samples, suggesting that urban dust derives from local rocks, b) Ni-V-Th*10 ternary diagram suggesting a felsic character for the rock samples and an intermediate character for the urban dust and Zn concentrate samples, c) TiO_2-Zr bivariate diagram providing additional evidence of the felsic origin of rock samples and intermediate origin of urban dust, and d) Zr/Ti vs. Nb/Y geochemical classification diagram supporting that all samples derived from felsic and intermediate sources, namely rhyolite-dacite, andesite, and trachyandesite and that urban dust derived from local rocks.

Figure 2b shows the Ni-V-Th*10 triangular diagram for rock, urban dust, and zinc concentrate samples. While rock samples were found near the Th axis, urban dust and zinc concentrate samples shifted to the V and Ni axes, respectively, suggesting that rock samples

derived from a felsic source such as the felsic-mafic local rocks (Torres-Sánchez et al., 2019), and urban dust and zinc concentrate samples derived from a more intermediate source. The high V concentrations found in the urban dust (Table S3, Supplementary material) suggested an enrichment of this element from anthropogenic sources. High V concentrations are known to derive from refineries, power plants, and the combustion of crude oil and its by-products (González-Guzmán et al., 2022; Moreno et al., 2010; Shafer et al., 2012; Silva et al., 2020).

Figure 2c shows the bivariate plot of TiO_2 vs. Zr for rock, urban dust, and zinc concentrate samples. The rock samples were consistently found in the field of felsic rocks, while urban dust samples were generally found in the field of intermediate rocks. These findings supported that rock samples derived from a felsic source, while urban dust samples derived from a more intermediate source.

Furthermore, Figure 2d presents the Zr/Ti vs. Nb/Y geochemical classification diagram for rock, urban dust, and zinc concentrate samples. Rock and zinc concentrate samples were predominantly categorized as rhyolites/dacites, andesites, and basaltic andesites, while urban dust samples were mostly classified as trachyandesite (Figure 2d), likely due to the higher Ti concentrations found in urban dust (Table S3, Supplementary Material), which, in turn, suggested an anthropogenic enrichment of Ti. Rutile, the most common form of TiO_2, is widely used in urban settings in paints, adhesives, plastics, and nanotechnology (Gallego-Hernández et al., 2020). The main types of rocks in the study area are rhyolitic and andesitic (Torres-Sánchez et al., 2019), while the Santa Bárbara and Charcas deposits comprise andesitic-rhyolitic and andesites (SGM, 1999, 2000), which explained the geochemical classification of rock and zinc concentrate samples and revealed that urban dust derived from the rocks present in the volcanic complex of the San Miguelito Mountain Range.

3.2. The geogenic or anthropogenic origin of PTE

Figure 3a shows the EF of urban dust showing the following enrichment: ΣREE<Sc<Zr<Sr<Fe<As<Mn<Cr<Pb<V<Zn<Cu. The mean EF for ΣREEs exhibited background concentrations (<1), Sc and Zr showed minimal enrichment (1-1.5), Sr, Fe, As, and Mn showed moderate enrichment (2-5), Cr, Pb, V, Zn showed significant enrichment (5-20), and Cu showed extremely high enrichment (>40). These findings indicated that urban dust in the SLPMA was anthropogenically enriched with As, Mn, Cr, Pb, V, Zn, and Cu. The enrichment of Zn, Cu, and Pb in urban dust from the SLPMA had previously been attributed to anthropogenic sources (Aguilera et al., 2019).

Figure 3b shows the PCA results, representing that PC1 and PC2 explaining 96% of the total data variability. PC1 (88%) was primarily composed of ΣREE, Sc, Zr, Sr, V, and Cr, while PC2 (8%) was mainly influenced by Fe. The PCA analysis showed a clear separation of the samples, from left to right, with rock samples (on the left), followed by urban dust (in the middle-right), and zinc concentrate samples (on the right) (Figure 3b). This shows that zinc concentrates were dominated by Zn, Cu, As, Pb, and Mn, while rocks were dominated by ΣREE, Sc, and Zr. Urban dust samples were dominated by Cr and V. Therefore, the enrichment of Zn, Cu, As, and Pb in urban dust samples was attributed to the presence of zinc concentrates. These findings were supported by cluster analysis, which grouped Zn, Cu, As, Pb, and Mn (from zinc concentrates), ΣREE, Sc, and Zr (from rock samples), and Cr, V, and Sr (from urban dust) (Figure S1, Supplementary Material).

Before 2010, high Pb and As concentrations in soils in SLPMA, as well as high Pb, Zn, Cu, and As in atmospheric particles, were attributed to the former copper and arsenic plants that were shut down in 2010 in the SLPMA (Carrizales et al., 2006; Piña et al., 2002). Recently, the

presence of Zn, Cu, and Pb in urban dust was attributed to the ZR in the SLPMA (Aguilera et al., 2019), oversighting the As contamination in urban dust as likely due to the shutdown of the copper and arsenic plants that used to release arsenolite (Martínez Jardines, 2018). For the very first time, we report the presence of As in urban dust in the SLPMA due to the impact of the ZR within the city, which showed a statistically significant positive relationship with Zn ($r=0.88$; $p<0.05$) (Table S5, Supplementary Material).

Since REEs are resistant to fractionation during sedimentation and weathering, PTEs from geogenic sources were expected to exhibit positive relationships with ΣREE, while PTEs from anthropogenic sources were expected to exhibit negative relationships with ΣREE (Dehghani et al., 2018; González-Guzmán et al., 2022; Moreno et al., 2006). The ΣREE concentration showed statistically significant positive correlations ($p<0.05$) with Sc ($r=0.99$), Sr ($r=0.77$), and Zr ($r=0.98$), while it showed statistically significant negative correlations ($p<0.05$) with Zn ($r=-0.91$), Cu ($r=-0.98$), Pb ($r=-0.94$), As (-0.75), and Mn ($r=-0.78$) (Table S5, Supplementary Material). Therefore, the enrichment of As, Mn, Pb, Cu, and Zn in urban dust was attributed to the zinc concentrate refinery process at SLPMA.

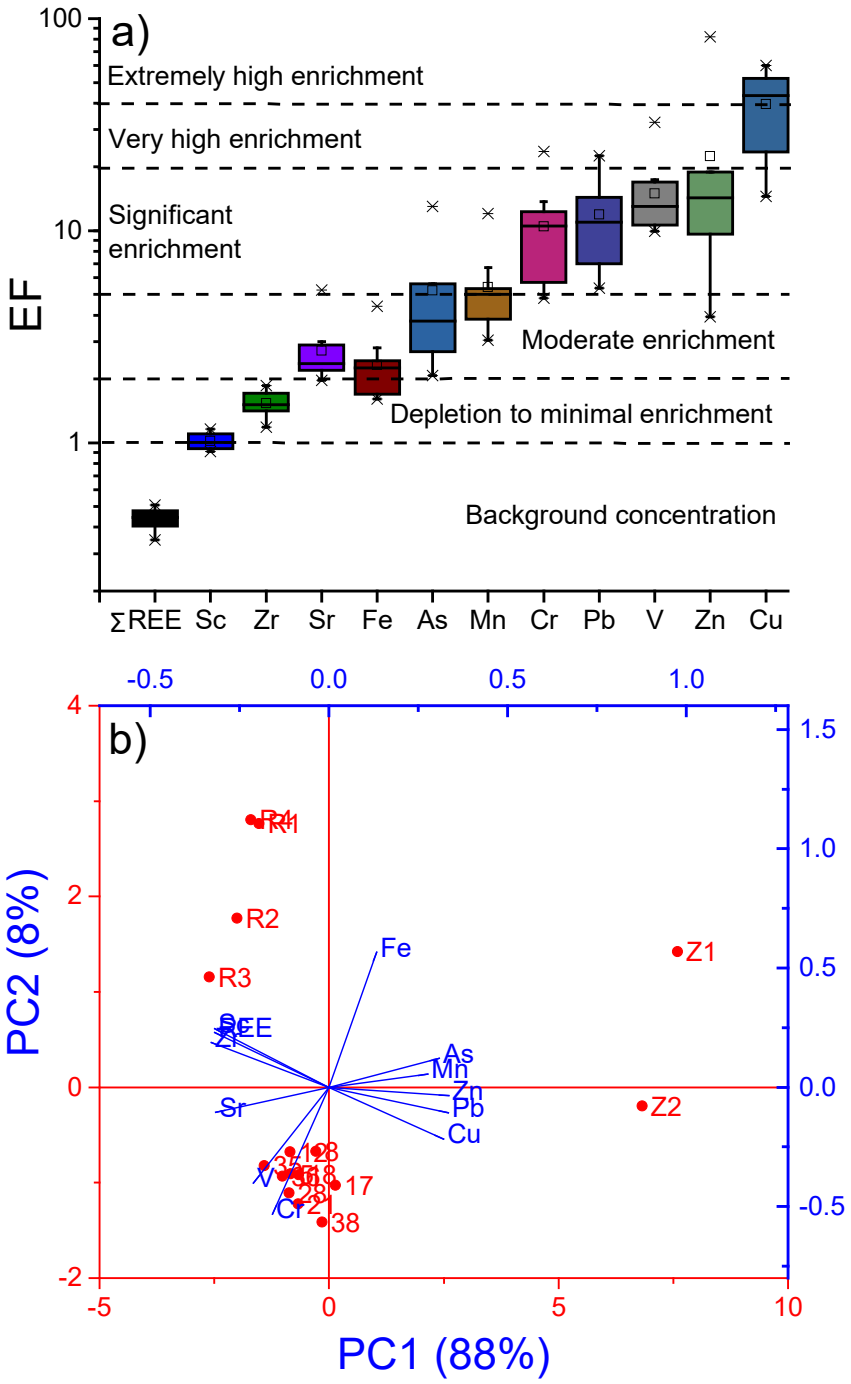

Figure 3. a) EFs in urban dust exhibiting moderate to extremely high enrichment for As, Mn, Cr, Pb, V, Zn, and Cu. b) PCA results showing PC1 and PC2, which explained 96% of the total variability of the data, as well as the contribution of each variable to each component. The geochemical variables are presented in red, while the samples are shown in black.

3.3. The sources of PTE

Figure 4a shows the 3.1*La-1.54*Ce-Zn ternary diagram depicting a line that started with rock samples (with crustal compositions between the 1.54*Ce and 3.1*La axes) and headed towards the Zn axis with urban dust samples followed by zinc concentrates. The urban dust samples closest to the ZR reached up to 90% of Zn composition, while the zinc concentrate samples showed nearly 100% of Zn composition, suggesting that the very high enrichment of Zn in urban dust samples derived from the ZR (Figures 3a and 4a).

Figure 4b showed the XRD pattern of zinc concentrates indicating sphalerite (ZnS) as the main mineral phase (80%), followed by domeykite (8.5%), chalcopyrite (6.8%), and galena (4%), providing additional chemical evidence of the impact of the ZR in urban dust.

Figure 4c show an elemental image of zinc concentrates revealing the presence of Zn, Pb, and As, while Figure 4d shows a SEM-EDS image of the characteristic elongated crystal morphology of sphalerite, which was also observed in urban dust collected at sampling point 8 (Figure 4e), near to the ZR (Figure 1). As mentioned previously, the ZR had been identified as a possible source of Zn particles in the urban dust of the SLPMA (Aguilera et al., 2019), but in this study, we have revealed that it contributes not only to urban dust enrichment with Zn, but also with Pb and As. Additionally the alternative research hypothesis tested significantly positive (p-value < 0.05) indicating that the integration of urban dust, geological, and pollution source samples, along with sound chemical analysis, accurately differentiated the geogenic and anthropogenic sources of PTE in urban dust (Table S6, Supplementary Material).

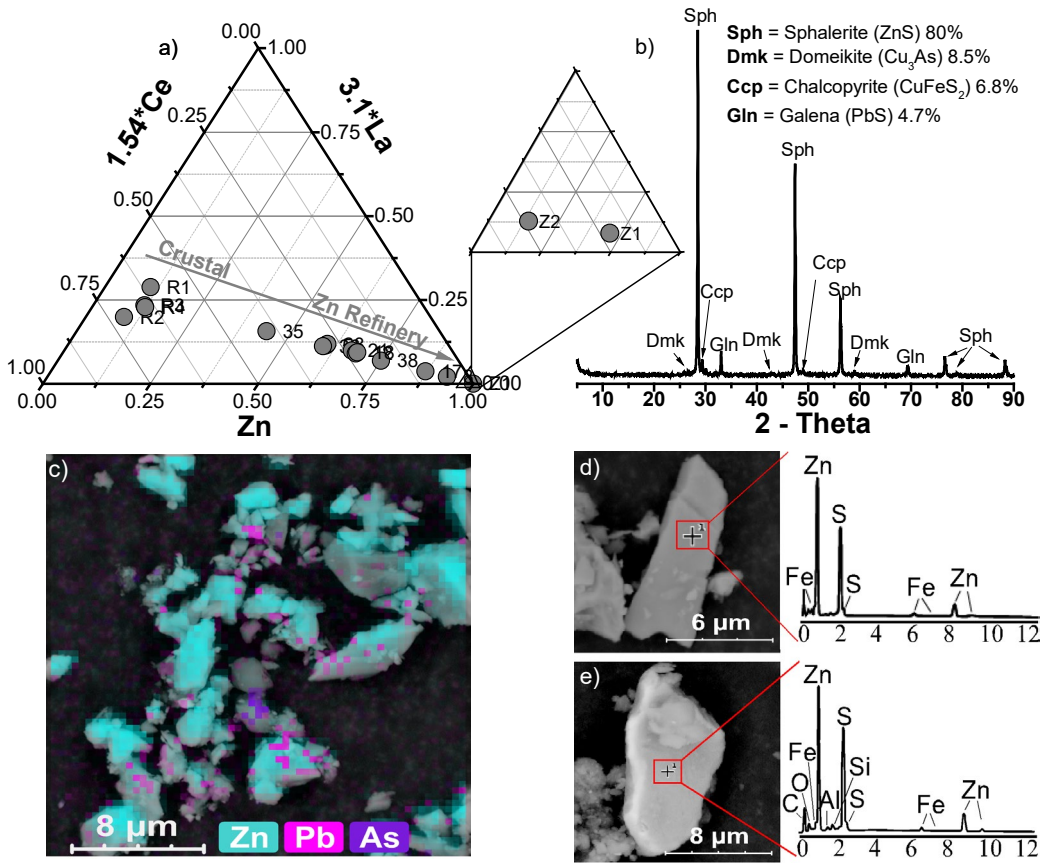

Figure 4. a) 3.1*La–1.54*Ce–Zn ternary diagram suggesting that the ZR was the source of Zn in urban dust samples, b) XRD diffractogram of zinc concentrates revealing the presence of sphalerite as the main mineral phase in zinc concentrates, c) elemental map of zinc concentrates revealing the presence of Pb (in pink), Zn (in blue), and As (in purple), d) SEM image and EDS spectra confirming the presence of sphalerite in zinc concentrates, and e) SEM image and EDS spectra showing the presence of sphalerite (most likely from the ZR) in urban dust sample 8 confirming therefore the source of Zn, Pb, and As (and maybe other PTEs) in urban dust is the ZR.

3.4. The spatial and seasonal distribution of PTE

Figure 5 shows the spatial and temporal distribution (pre and post rainy season) of Zn, As and Pb in urban dust samples. Zinc concentrations ranged from <800 to 20,008 mg/kg, As concentrations ranged from <22 to 284 mg/kg, and Pb concentrations ranged between <85 and 776 mg/kg. The western zone of the SLPMA (that included the U2, U3, and U5 urban basins and the ZR exhibited higher concentrations of Zn (>5000 mg/kg), As (>120 mg/kg), and Pb (>400 mg/kg)

(Figure 5). The spatial and temporal distributions of Zn, As, and Pb were very similar, except for in the southeast area (that included the U7, U8, and U9 urban basins and the SLPMA industrial zone), which exhibited high concentrations of Pb (Figure 5). In the pre rainy season sampling, the distributions of Zn, As, and Pb were primarily to the northeast, east, and south of the ZR, while in the post rainy season sampling, it shifted towards the east of the ZR, which was likely due to prevailing wind directions (Figure 5h and i). In addition, topography could influence the spatial distribution of Zn, As, and Pb, since their concentrations spread from the ZR towards lower elevation areas (Figure 5g), mainly during post sampling (Figure 5), which could be explained by runoff surface during the surface runoff. The spatial distributions of Zn and Pb found in this study were consistent with previous findings in urban dust from the SLPMA (Aguilera et al., 2019). Previous studies attributed the high concentrations of Pb in atmospheric particles from the SLPMA to emissions from the industrial zone of the area (Aragón-Piña et al., 2006).

Currently, standards for maximum permissible levels of PTEs in urban dust are nonexistent worldwide. However, Mexican guidelines account for a maximum permissible level of 22 mg/kg of As and 400 mg/kg of Pb in residential or commercial soils (DOF, 2007), while Canadian soil quality guidelines establish a maximum of 250 mg/kg of Zn for residential soils and 410 mg/kg for commercial and industrial soils (CCME, 2018). Arsenic and Zn concentrations in urban dust in SLPMA exceeded the guidelines throughout the city, indicating that contamination derived from the ZR, while Pb exceeded the permissible limits in the west and southeast (Figure 5), indicating that contamination derived from the industrial area. Studies around zinc refineries have mainly focused on determining PTEs in soil (Liu et al., 2023; Zeng et al., 2022), while little attention has been paid to PTEs in dust (Zheng et al., 2010). To the extent of our knowledge, this is the first study to report As contamination in urban dust resulting from a zinc refinery. The spatial and

temporal distributions of Cu, Mn, Cr, V, Sr, and Fe, exhibited no clear patterns (Figures S3 and S4, Supplementary Material), suggesting that these PTEs may derive from multiple sources or non-point sources. Significant differences ($p<0.05$) were not found in PTE concentrations between pre and post rainy season sampling (Table S7, Supplementary Material), indicating that the continuous year-round operation of the ZR might surpass any seasonal effect reported in other studies (Schiavo et al., 2021).

423

424 **Figure 5.** Spatial distribution of Zn, As, and Pb in urban dust samples (n=38), pre and post rainy, revealing high
425 concentrations of Zn, As and Pb in urban dust in western SLPMA likely due to the presence of a ZR and high
426 concentrations of Pb in south-east SLPMA, probably due to industrial activity.

3.5. Health risk

Figure 6a shows the particle size distribution of $PM_{2.5}$, $PM_{5.0}$, PM_{10}, and PM_{20} in urban dust samples, ranging from 66 to 84%, 13 to 27%, 3 to 8%, and 0 to 2%, respectively, revealing that the most abundant particles were <2.5 μm and highlighting a risk of inhalation to deep parts of the lung (such as the secondary bronchi and pulmonary alveoli). Potential population health consequences include exacerbation of asthma, reduced lung function, airway irritation, coughing, shortness of breath, lung cancer, and premature death in people with heart or lung disease (EPA, 2022). Figure 6b shows the lung bioaccessibility of Sr, Zn, Cu, Fe, and Mn, ranging from 48.5 to 72.4%, 9.6 to 28.4%, 10.5 to 27.0%, 4.5 to 8.6%, and 2.9 to 28.4%, respectively, revealing that Sr, Zn, Fe, Cu, Mn, Cr (38.3% in sample 38), and Pb (30.6% in sample 38 after the rainy season) may dissolve in pulmonary fluids, absorb in the bloodstream, and cause systemic toxicity (Innes et al., 2021). While Sr is beneficial for bone health, its inhalation could result in severe respiratory distress, anaphylactic reactions, and extreme tachycardia (Qu et al., 2012). Sr can also substitute Ca in organisms, inhibit normal Ca absorption, cause bone damage, anemia, oxygen deprivation, and even cancer due to damage to the genetic material of cells (Pathak et al., 2020). Although Zn is an essential element, inhalation and bioaccessibility of zinc particles has not been extensively studied and there is limited data on its effects on health. Some studies have shown that inhalation of ZnO can cause lung inflammation and oxidative stress (Fukui et al., 2012). In addition, it has been linked to degenerative diseases of the nervous system and may contribute to the formation of degenerative plaques in the brain of Alzheimer's patients (Plumlee & Ziegler, 2007). The bioaccessibility of As, V, and Zr was below the detection limit in both samplings, and Sc was not determined. Prolonged exposure combined with high lung burden of bio-durable particles (i.e., particles that are insoluble or poorly soluble in body fluids) can lead to macrophage dysfunction

and increased particle transfer to lymph nodes, chronic lung inflammation, epithelial cell proliferation, and fibrosis (Borm et al., 2015; Cullen et al., 2000; Plumlee & Ziegler, 2007). Significant differences ($p < 0.05$) in particle size count and lung bioaccessibility between pre and post rainy season sampling were not found (Table S7, Supplementary Material).

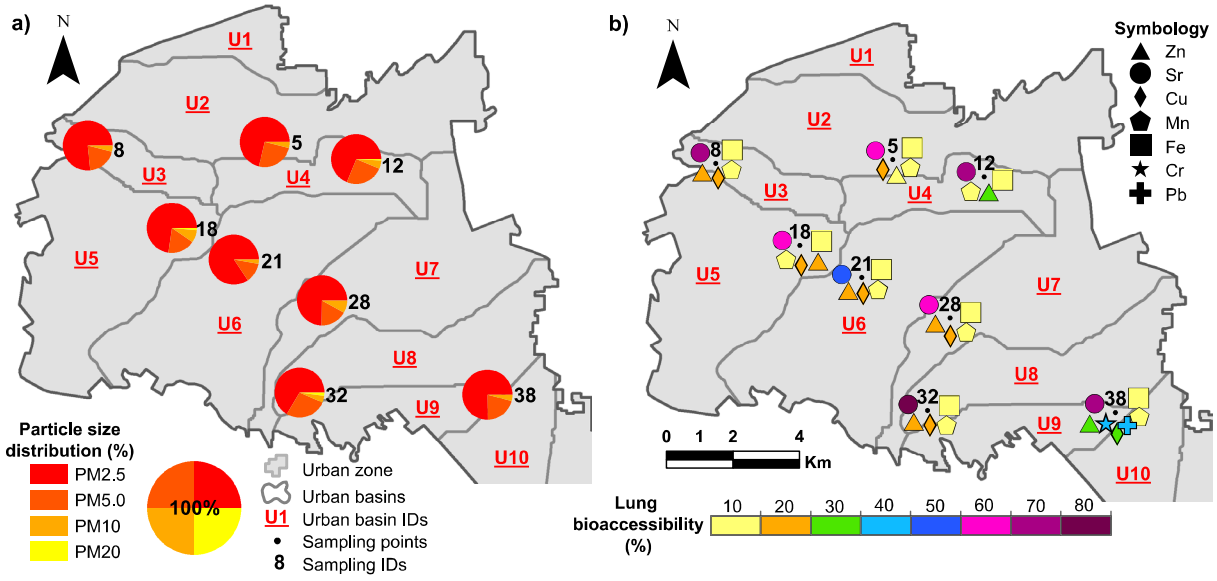

Figure 6. a) Particle size distribution of urban dust and b) lung bioaccessibility of Zn, Sr, Cu, Mn, Fe, Cr, and Pb.

This research proposes a new alternative for the characterization of urban dust and the precise identification of the source of origin through the integration of sampling and chemical analysis. Sampling is a critical phase that must be carried out carefully. For this work, sampling points were defined considering the study area's physiographic aspects and essential elements such as the prevailing wind direction, the detection of runoff accumulation areas, and the identification of natural/anthropogenic sources as reference elements. These elements were crucial for adequately characterizing the study area to establish representative sampling points. Another aspect to consider was the number of sampling points. The idea was to have as many samples as possible,

but in practice, sampling in an urban area, where the dynamics of the city (pedestrian and vehicular traffic, cleaning up, and urban maintenance services, among others) do not guarantee the collection of an intact sample, but rather one that its environment has modified. Given this situation, in this study, we chose strategic sampling points to cover the territorial extension of SLPMA. We identified the ZR as the source of Zn, As, and Pb in SLPMA, but other emission sources for PTEs might exist. A thorough identification would need samples from different emission points. Future work will expand the monitoring network to increase the coherence and significance of the data obtained in this research project. It's also important to note that our focus was solely on one central Mexican city, which may not represent the varied urban settings and emission sources elsewhere. Expanding this study to encompass multiple cities with various industrial activities and geological settings would contribute to a more robust generalization of the findings.

4. Conclusions

Multivariate statistical analyses and documentary information are commonly used to discern the geogenic or anthropogenic origins of PTEs in urban dust. Although they are powerful tools for grouping PTEs into emission source types with similar chemical profiles, they cannot always provide accurate identification of a pollutant's point source, such as a specific industry. The limitations of these approaches arise due to the restricted availability of geochemical data derived solely from urban dust samples. This study used a comprehensive approach that combined multiple techniques and methodologies to analyze samples from urban dust, rocks, and emission sources. REE concentrations and geochemical diagrams (Ni-V-Th*10, TiO2-Zr, Zr/Ti vs. Nb/Y) were practical tools to determine the provenance of urban dust. Discrimination between the geogenic and anthropogenic origin of PTEs in urban dust was determined from PTE concentrations, enrichment factor (EF), and CoDA analyses. Sound chemical and classic geochemical tools such as a modified version of the 3.1*La-1.54*Ce-V geochemical diagram, mineralogy, elemental composition, and mineral morphology helped to strengthen the methodology and improve the detection of the point emission source of Zn, As, and Pb. After the origin of PTEs in urban dust was identified, the spatial representation of the results allowed us to identify broader areas of risk, both territorially and temporally, where urban dust transport due to seasonal precipitation and wind direction could be observed, establishing a more dynamic behavior than what was provided at the beginning of the investigation. Finally, this research provided valuable information on the potential health risks of PTEs due to particle size and pulmonary bioaccessibility. The results of this study contribute to a better understanding of environmental issues in urban systems, which are of global concern, given that more than 55% of the world's population currently lives in urban areas, and this figure is expected to increase to 68% by 2050.

Acknowledgements

The authors thank M.Sc. Beatriz Adriana Escoto from LINAN at IPICYT, Dr. Belem Gonzalez-Grijalva from LANGEM at UNISON, Dr. Héctor Hernández Mendoza from LAMA at UCEM and Instituto de Investigación de Zonas Desérticas at UASLP. M.Sc. Jesus Piña-Leyte-Vidal from IPICYT. R.R. is thankful to CONACYT for Ph.D. scholarship No. 861430 and N.M.V. is thankful to CONACYT for Grant No. 7073, the Newton Fund/Royal Society (NA140182), and the Newton Fund/British Council-COPOCYT (629008622). DMF is thankful to CONACYT for Grant No. 317557. Many thanks to Lucy Rose McKenna for the English revisions.

5. References

Aguilera, A., Armendariz, C., Quintana, P., García-Oliva, F., & Bautista, F. (2019). Influence of land use and road type on the elemental composition of urban dust in a Mexican Metropolitan Area. *Polish Journal of Environmental Studies*, *28*(3), 1535–1547. https://doi.org/10.15244/pjoes/90358

Aguillón-Robles, A., Tristán-González, M., Aguirre-Díaz, G. de J., López-Doncel, R. A., Bellon, H., & Martínez-Esparza, G. (2014). Eocene to Quaternary mafic-intermediate volcanism in San Luis Potosí, central Mexico: The transition from Farallon plate subduction to intra-plate continental magmatism. *Journal of Volcanology and Geothermal Research*, *276*, 152–172. https://doi.org/https://doi.org/10.1016/j.jvolgeores.2014.02.019

Aguillón-Robles, A., Tristán-González, M., López-Doncel, R. A., García-Arreola, M. E., Almaguer-Rodríguez, J. de L., & Maury, R. C. (2012). Trace elements geochemistry and origin of volcanic units from the San Luis Potosí and Río Santa María volcanic fields, Mexico: the bearing of ICP-QMS data. *Geofísica Internacional*, *51*(3), 293–308. http://www.scielo.org.mx/scielo.php?script=sci_arttext&pid=S0016-71692012000300007&lng=es&nrm=iso&tlng=en

Aragón-Piña, A., Campos-Ramos, A. A., Leyva-Ramos, R., Hernández-Orta, M., Miranda-Ortiz, N., & Luszczewski-Kudra, A. (2006). Influencia de emisiones industriales en el polvo atmosférico de la ciudad de San Luis Potosí, México. *Revista Internacional de Contaminación Ambiental*, *22*(1), 5–15. http://www.scielo.org.mx/scielo.php?script=sci_arttext&pid=S0188-49992006000100005&lng=es&nrm=iso&tlng=es

Arruda, D. L. de, Ker, J. C., Schaefer, C. E., Melo, H. F. de, Camêlo, D. de L., Paes, É. de C., & Barroso, S. H. (2023). Unraveling the sedimentation environment of Marajó island: Insights

from geochemical studies and implications for the origin of potentially toxic element in soils. *Journal of South American Earth Sciences*, *128*, 104452. https://doi.org/https://doi.org/10.1016/j.jsames.2023.104452

Barboza Gudiño, R. (2018). *Actualización del atlas de riesgo para el municipio de San Luis Potosí y su zona conurbada*. Universidad Autónoma de San Luis Potosí / Instituto de Geología. https://sanluisimplan.gob.mx/wp-content/uploads/programas_2021/atlas.pdf

Bern, C. R., Walton-Day, K., & Naftz, D. L. (2019). Improved enrichment factor calculations through principal component analysis: Examples from soils near breccia pipe uranium mines, Arizona, USA. *Environmental Pollution*, *248*, 90–100. https://doi.org/10.1016/J.ENVPOL.2019.01.122

Borm, P., Cassee, F. R., & Oberdörster, G. (2015). Lung particle overload: old school –new insights? *Particle and Fibre Toxicology*, *12*(1), 10. https://doi.org/10.1186/s12989-015-0086-4

Bourliva, A., Kantiranis, N., Papadopoulou, L., Aidona, E., Christophoridis, C., Kollias, P., Evgenakis, M., & Fytianos, K. (2018). Seasonal and spatial variations of magnetic susceptibility and potentially toxic elements (PTEs) in road dusts of Thessaloniki city, Greece: A one-year monitoring period. *Science of The Total Environment*, *639*, 417–427. https://doi.org/10.1016/J.SCITOTENV.2018.05.170

Bracciali, L., Marroni, M., Luca, P., & Sergio, R. (2007). Geochemistry and petrography of western Tethys Cretaceous sedimentary covers (Corsica and Northern Apennines): From source areas to configuration of margins. In J. Arribas, M. J. Johnsson, & S. Critelli (Eds.), *Sedimentary provenance and petrogenesis: perspectives from petrography and geochemistry* (Vol. 420, pp. 73–93). The Geological Society of America Special Papers. https://doi.org/10.1130/2006.2420(06)

Carrizales, L., Razo, I., Téllez-Hernández, J. I., Torres-Nerio, R., Torres, A., Batres, L. E., Cubillas, A.-C., & Díaz-Barriga, F. (2006). Exposure to arsenic and lead of children living near a copper-smelter in San Luis Potosi, Mexico: Importance of soil contamination for exposure of children. *Environmental Research*, *101*(1), 1–10. https://doi.org/10.1016/j.envres.2005.07.010

CCME. (2018). Canadian soil quality guidelines for the protection of environmental and human health: Zinc 2018. In *Canadian Council of Ministers of the Environment*. Canadian environmental quality guidelines. https://ccme.ca/en/res/zinc-canadian-soil-quality-guidelines-for-the-protection-of-environmental-and-human-health-en.pdf

Choobari, O. A., Zawar-Reza, P., & Sturman, A. (2014). The global distribution of mineral dust and its impacts on the climate system: A review. *Atmospheric Research*, *138*, 152–165. https://doi.org/10.1016/j.atmosres.2013.11.007

Colombo, C., Monhemius, A. J., & Plant, J. A. (2008). Platinum, palladium and rhodium release from vehicle exhaust catalysts and road dust exposed to simulated lung fluids.

Ecotoxicology and Environmental Safety, *71*(3), 722–730. https://doi.org/https://doi.org/10.1016/j.ecoenv.2007.11.011

CONAGUA. (2018). *Informe de precipitaciones diarias, mensuales y anuales en SLP 1980-2018.*

CONAGUA. (2019). *Dirección y velocidad del viento SLP (SAN LUIS POTOSI - OBS) 1980-2018*.

Cullen, R. T., Tran, C. L., Buchanan, D., Davis, J. M., Searl, A., Jones, A. D., & Donaldson, K. (2000). Inhalation of poorly soluble particles. I. Differences in inflammatory response and clearance during exposure. *Inhalation Toxicology*, *12*(12), 1089–1111. https://doi.org/10.1080/08958370050166787

Dehghani, S., Moore, F., Vasiluk, L., & Hale, B. A. (2018). The geochemical fingerprinting of geogenic particles in road deposited dust from Tehran metropolis, Iran: Implications for provenance tracking. *Journal of Geochemical Exploration*, *190*, 411–423. https://doi.org/10.1016/j.gexplo.2018.04.011

DOF. (2007). *NORMA Oficial Mexicana NOM-147-SEMARNAT/SSA1-2004, Que establece criterios para determinar las concentraciones de remediación de suelos contaminados por arsénico, bario, berilio, cadmio, cromo hexavalente, mercurio, níquel, plata, plomo, selenio, talio y/o vanadio.* Secretaría de Medio Ambiente y Recursos Naturales, Diario Oficial de la Federación. México. https://www.profepa.gob.mx/innovaportal/file/1392/1/nom-147-semarnat_ssa1-2004.pdf

EPA. (2014). *Method 6020B (SW-846): Inductively Coupled Plasma - Mass Spectrometry*. United States Environmental Protection Agency. Washington, DC. https://www.epa.gov/esam/epa-method-6020b-sw-846-inductively-coupled-plasma-mass-spectrometry

EPA. (2022, August 30). *Health and environmental effects of particulate matter (PM), health effects*. U.S. Environmental Protection Agency. https://www.epa.gov/pm-pollution/health-and-environmental-effects-particulate-matter-pm

Fan, P., Lu, X., Yu, B., Fan, X., Wang, L., Lei, K., Yang, Y., Zuo, L., & Rinklebe, J. (2022). Spatial distribution, risk estimation and source apportionment of potentially toxic metal(loid)s in resuspended megacity street dust. *Environment International*, *160*, 107073. https://doi.org/10.1016/j.envint.2021.107073

Fukui, H., Horie, M., Endoh, S., Kato, H., Fujita, K., Nishio, K., Komaba, L. K., Maru, J., Miyauhi, A., Nakamura, A., Kinugasa, S., Yoshida, Y., Hagihara, Y., & Iwahashi, H. (2012). Association of zinc ion release and oxidative stress induced by intratracheal instillation of ZnO nanoparticles to rat lung. *Chemico-Biological Interactions*, *198*(1–3), 29–37. https://doi.org/10.1016/j.cbi.2012.04.007

606 Gaberšek, M., Watts, M. J., & Gosar, M. (2022). Attic dust: an archive of historical air
607 contamination of the urban environment and potential hazard to health? *Journal of*
608 *Hazardous Materials*, *432*, 128745. https://doi.org/10.1016/J.JHAZMAT.2022.128745

609 Gallego-Hernández, A. L., Meza-Figueroa, D., Tanori, J., Acosta-Elías, M., González-Grijalva,
610 B., Maldonado-Escalante, J. F., Rochín-Wong, S., Soto-Puebla, D., Navarro-Espinoza, S.,
611 Ochoa-Contreras, R., & Pedroza-Montero, M. (2020). Identification of inhalable rutile and
612 polycyclic aromatic hydrocarbons (PAHs) nanoparticles in the atmospheric dust.
613 *Environmental Pollution*, *260*, 114006. https://doi.org/10.1016/j.envpol.2020.114006

614 González Medrano, F. (2012). *Las zonas áridas y semiáridas de México y su vegetación* (1st
615 ed.). Secretaría de Medio Ambiente y Recursos Naturales, Instituto Nacional de Ecología.
616 http://140.84.163.2:8080/xmlui/bitstream/handle/publicaciones/218/668_2012_Zonas_arida
617 s_semiaridas_Mexico.pdf?sequence=1&isAllowed=y

618 González-Guzmán, R., Inguaggiato, C., Brusca, L., González-Acevedo, Z. I., & Bernard-
619 Romero, R. (2022). Assessment of potentially toxic elements (PTEs) sources on soils
620 surrounding a fossil fuel power plant in a semi-arid/arid environment: A case study from the
621 Sonoran Desert. *Applied Geochemistry*, *136*, 105158.
622 https://doi.org/10.1016/j.apgeochem.2021.105158

623 Guney, M., Bourges, C. M.-J., Chapuis, R. P., & Zagury, G. J. (2017). Lung bioaccessibility of
624 As, Cu, Fe, Mn, Ni, Pb, and Zn in fine fraction (<20μm) from contaminated soils and mine
625 tailings. *Science of The Total Environment*, *579*, 378–386.
626 https://doi.org/https://doi.org/10.1016/j.scitotenv.2016.11.086

627 Haung, C.-C., Cai, L., Xu, Y.-H., Wen, H.-H., Luo, J., Hu, G.-C., Chen, L.-G., Wang, H.-Z., Xu,
628 X.-B., & Mei, J.-X. (2022). Quantitative analysis of ecological risk and human health risk
629 of potentially toxic elements in farmland soil based on PMF model. *Land Degradation and*
630 *Development* , *33*(11), 1954–1967. https://doi.org/10.1002/ldr.4277

631 Hayashi, K.-I., Fujisawa, H., Holland, H. D., & Ohmoto, H. (1997). Geochemistry of ~1.9 Ga
632 sedimentary rocks from northeastern Labrador, Canada. *Geochimica et Cosmochimica Acta*,
633 *61*(19), 4115–4137. https://doi.org/10.1016/S0016-7037(97)00214-7

634 Ho, H. H., Swennen, R., Cappuyns, V., Vassilieva, E., & Van Tran, T. (2012). Necessity of
635 normalization to aluminum to assess the contamination by heavy metals and arsenic in
636 sediments near Haiphong Harbor, Vietnam. *Journal of Asian Earth Sciences*, *56*, 229–239.
637 https://doi.org/10.1016/J.JSEAES.2012.05.015

638 Huang, C.-C., Cai, L.-M., Xu, Y.-H., Jie, L., Chen, L.-G., Hu, G.-C., Jiang, H.-H., Xu, X.-B., &
639 Mei, J.-X. (2022). A comprehensive exploration on the health risk quantification assessment
640 of soil potentially toxic elements from different sources around large-scale smelting area.
641 *Environmental Monitoring and Assessment*, *194*(3), 206. https://doi.org/10.1007/s10661-
642 022-09804-0

643 Huang, C.-C., Cai, L.-M., Xu, Y.-H., Jie, L., Hu, G.-C., Chen, L.-G., Wang, H.-Z., Xu, X.-B., &
644 Mei, J.-X. (2023). A comprehensive approach to quantify the source identification and
645 human health risk assessment of toxic elements in park dust. *Environmental Geochemistry*
646 *and Health*, *45*(8), 5813–5827. https://doi.org/10.1007/s10653-023-01588-7

647 Huyan, Y., & Yao, W. (2022). Geochemical comparisons of weathering, provenance and
648 tectonics in the fluvial sediments from Yarlung Zangbo to Brahmaputra River. *CATENA*,
649 *210*, 105944. https://doi.org/10.1016/j.catena.2021.105944

650 INEGI. (2021). *Panorama sociodemográfico de San Luis Potosí: Censo de Población y Vivienda*
651 *2020* (México : INEGI c2021). Aguascalientes, Instituto de Estadística y Geografía, p.141.

652 Innes, E., Yiu, H. H. P., McLean, P., Brown, W., & Boyles, M. (2021). Simulated biological
653 fluids – a systematic review of their biological relevance and use in relation to inhalation
654 toxicology of particles and fibres. *Critical Reviews in Toxicology*, *51*(3), 217–248.
655 https://doi.org/10.1080/10408444.2021.1903386

656 Kastury, F., Smith, E., Karna, R. R., Scheckel, K. G., & Juhasz, A. L. (2018). Methodological
657 factors influencing inhalation bioaccessibility of metal(loid)s in PM2.5 using simulated lung
658 fluid. *Environmental Pollution*, *241*, 930–937.
659 https://doi.org/https://doi.org/10.1016/j.envpol.2018.05.094

660 Lima, L. H. V., do Nascimento, C. W. A., da Silva, F. B. V., & Araújo, P. R. M. (2023). Baseline
661 concentrations, source apportionment, and probabilistic risk assessment of heavy metals in
662 urban street dust in Northeast Brazil. *Science of The Total Environment*, *858*, 159750.
663 https://doi.org/10.1016/j.scitotenv.2022.159750

664 Liu, Y., Qiao, J., & Sun, Y. (2023). Enhanced immobilization of lead, cadmium, and arsenic in
665 smelter-contaminated soil by sulfidated zero-valent iron. *Journal of Hazardous Materials*,
666 *447*, 130783. https://doi.org/10.1016/J.JHAZMAT.2023.130783

667 Ma, L., Wu, J., Abuduwaili, J., & Liu, W. (2016). Geochemical responses to anthropogenic and
668 natural influences in Ebinur Lake sediments of arid northwest China. *PLoS One*, *11*(5),
669 e0155819. https://doi.org/10.1371/journal.pone.0155819

670 Mair, P., & Wilcox, R. (2020). *Robust statistical methods in R using the WRS2 Package.*
671 *Behavior research methods*. Harvard University and University of Southern California.
672 https://cran.r-project.org/web/views/Robust.html

673 Martínez Jardines, L. G. (2018). *Barreras geoquímicas y estabilización físico-química para el*
674 *manejo ambientalmente seguro de residuos metalúrgicos y suelos contaminados con*
675 *arsénico y metales pesados en San Luis Potosí.* [Tesis de doctorado, Universidad Nacional
676 Autónoma de México]. http://132.248.9.195/ptd2018/abril/0773129/0773129.pdf

677 Merli, M., Bonadiman, C., & Pavese, A. (2020). Aluminium distribution in an Earth's non–
678 primitive lower mantle. *Geochimica et Cosmochimica Acta*, *276*, 70–91.
679 https://doi.org/10.1016/J.GCA.2020.02.023

Meza-Figueroa, D., Barboza-Flores, M., Romero, F. M., Acosta-Elias, M., Hernández-Mendiola, E., Maldonado-Escalante, F., Pérez-Segura, E., González-Grijalva, B., Meza-Montenegro, M., García-Rico, L., Navarro-Espinoza, S., Santacruz-Gómez, K., Gallego-Hernández, A., & Pedroza-Montero, M. (2020). Metal bioaccessibility, particle size distribution and polydispersity of playground dust in synthetic lysosomal fluids. *Science of The Total Environment*, *713*, 136481. https://doi.org/10.1016/j.scitotenv.2019.136481

Meza-Figueroa, D., De la O-Villanueva, M., & De la Parra, M. L. (2007). Heavy metal distribution in dust from elementary schools in Hermosillo, Sonora, México. *Atmospheric Environment*, *41*(2), 276–288. https://doi.org/10.1016/J.ATMOSENV.2006.08.034

Meza-Figueroa, D., González-Grijalva, B., Romero, F., Ruiz, J., Pedroza-Montero, M., Rivero, C. I.-D., Acosta-Elías, M., Ochoa-Landin, L., & Navarro-Espinoza, S. (2018). Source apportionment and environmental fate of lead chromates in atmospheric dust in arid environments. *Science of The Total Environment*, *630*, 1596–1607. https://doi.org/10.1016/j.scitotenv.2018.02.285

Moreno, T., Querol, X., Alastuey, A., de la Rosa, J., Sánchez de la Campa, A. M., Minguillón, M., Pandolfi, M., González-Castanedo, Y., Monfort, E., & Gibbons, W. (2010). Variations in vanadium, nickel and lanthanoid element concentrations in urban air. *Science of The Total Environment*, *408*(20), 4569–4579. https://doi.org/10.1016/j.scitotenv.2010.06.016

Moreno, T., Querol, X., Alastuey, A., & Gibbons, W. (2008). Identification of FCC refinery atmospheric pollution events using lanthanoid- and vanadium-bearing aerosols. *Atmospheric Environment*, *42*(34), 7851–7861. https://doi.org/10.1016/j.atmosenv.2008.07.013

Moreno, T., Querol, X., Castillo, S., Alastuey, A., Cuevas, E., Herrmann, L., Mounkaila, M., Elvira, J., & Gibbons, W. (2006). Geochemical variations in aeolian mineral particles from the Sahara–Sahel Dust Corridor. *Chemosphere*, *65*(2), 261–270. https://doi.org/10.1016/j.chemosphere.2006.02.052

Moreno-Rodríguez, V., Del Rio-Salas, R., Adams, D. K., Ochoa-Landin, L., Zepeda, J., Gómez-Alvarez, A., Palafox-Reyes, J., & Meza-Figueroa, D. (2015). Historical trends and sources of TSP in a Sonoran desert city: Can the North America Monsoon enhance dust emissions? *Atmospheric Environment*, *110*, 111–121. https://doi.org/10.1016/j.atmosenv.2015.03.049

Ortega Montoya, C. Y., Avila Galarza, A., Briones-Gallardo, R., Razo Soto, I., & Cerda, R. (2014). Differences in the risk profiles and risk perception of flammable liquid hazards in San Luis Potosi, Mexico. *Case Studies in Fire Safety*, *2*, 37–44. https://doi.org/10.1016/j.csfs.2014.10.002

Pathak, P., Srivastava, R. R., Keceli, G., & Mishra, S. (2020). Assessment of the Alkaline Earth Metals (Ca, Sr, Ba) and Their Associated Health Impacts. In P. Pathak & D. K. Gupta (Eds.), *Strontium Contamination in the Environment* (pp. 227–243). Springer International Publishing. https://doi.org/10.1007/978-3-030-15314-4_12

718 Pearce, J. A. (1996). A user's guide to basalt discrimination diagrams. In W. D.A. (Ed.), *Trace*
719 *Element Geochemistry of volcanic rocks: Applications for massive sulphide exploration*
720 (Short Course Notes, Vol. 12, pp. 79–113). Geological Association of Canada.
721 https://gac.ca/product/trace-element-geochemistry-of-volcanic-rocks-applications-for-
722 massive-sulphide-exploration/

723 Pelfrêne, A., Cave, M. R., Wragg, J., & Douay, F. (2017). In vitro investigations of human
724 bioaccessibility from reference materials using simulated lung fluids. *International Journal*
725 *of Environmental Research and Public Health*, *14*(2), 112.
726 https://doi.org/10.3390/ijerph14020112

727 Pereira, D. C. A., Custódio, D., de Andrade, M. de F., Alves, C., & de Castro Vasconcellos, P.
728 (2019). Air quality of an urban school in São Paulo city. *Environmental Monitoring and*
729 *Assessment*, *191*(11), 659. https://doi.org/10.1007/s10661-019-7815-3

730 Piña, A. A., Villaseñor, G. T., Jacinto, P. S., & Fernández, M. M. (2002). Scanning and
731 transmission electron microscope of suspended lead-rich particles in the air of San Luis
732 Potosi, Mexico. *Atmospheric Environment*, *36*(33), 5235–5243.
733 https://doi.org/10.1016/S1352-2310(02)00588-5

734 Plumlee, G. S., & Ziegler, T. L. (2007). The medical geochemistry of dusts, soils, and other earth
735 materials. In H. D. Holland & K. K. Turekian (Eds.), *Treatise on Geochemistry* (First
736 (Online), Vol. 9, pp. 1–61). Elsevier. https://doi.org/10.1016/B0-08-043751-6/09050-2

737 Qu, K., Zhao, C., Ren, J., & Qu, X. (2012). Human telomeric G-quadruplex formation and
738 highly selective fluorescence detection of toxic strontium ions. *Molecular BioSystems*, *8*(3),
739 779–782. https://doi.org/10.1039/c2mb05446a

740 R Core Team. (2023). *A language and environment for statistical computing. R Foundation for*
741 *Statistical Computing*. Vienna, Austria. https://www.r-project.org/

742 Revelle, W. (2021). *psych: Procedures for personality and psychological research* (2.3.3).
743 Northwestern University. https://CRAN.R-project.org/package=psych

744 Rodríguez Rodríguez, R. M. (2020). *Elementos potencialmente tóxicos en el polvo urbano de la*
745 *zona metropolitana de San Luis Potosí.* [Tesis de maestría, Instituto Potosino de
746 Investigación Científica y Tecnológica].
747 https://repositorio.ipicyt.edu.mx///handle/11627/5279

748 Sappa, G., Barbieri, M., & Andrei, F. (2020). Assessment of trace elements natural enrichment in
749 topsoil by some Italian case studies. *SN Applied Sciences*, *2*(8), 1409.
750 https://doi.org/10.1007/s42452-020-03214-y

751 Schiavo, B., Meza-Figueroa, D., Pedroza-Montero, M., Vidal-Solano, J., González-Grijalva, B.,
752 Navarro-Espinoza, S., Romero, F., Hernández, E., Gutiérrez-Ruiz, M. E., & Ceniceros-
753 Gómez, A. E. (2021). In vitro assessment oral and respiratory bioaccessibility of Mn in
754 school dust: Insight of seasonality in a semiarid environment. *Applied Geochemistry*, *134*,
755 105102. https://doi.org/10.1016/j.apgeochem.2021.105102

SGM. (1998). *Carta Geológico–Minera: San Luis Potosí F14-4*. http://mapserver.sgm.gob.mx/Cartas_Online/geologia/75_F14-4_GM.pdf

SGM. (1999). *Carta Geológico–Minera: Santa Barbara G13-A57*. Servicio Geológico Méxicano. http://mapserver.sgm.gob.mx/Cartas_Online/geologia/760_G13-A57_GM.pdf

SGM. (2000). *Carta Geológico–Minera: Charcas F14-A43*. Servicio Geológico Méxicano. http://mapserver.sgm.gob.mx/Cartas_Online/geologia/1408_F14-A43_GM.pdf

Shafer, M. M., Toner, B. M., Overdier, J. T., Schauer, J. J., Fakra, S. C., Hu, S., Herner, J. D., & Ayala, A. (2012). Chemical speciation of vanadium in particulate matter emitted from diesel vehicles and urban atmospheric aerosols. *Environmental Science & Technology*, *46*(1), 189–195. https://doi.org/10.1021/es200463c

Silva, L. F. O., Pinto, D., Neckel, A., & Oliveira, M. L. S. (2020). An analysis of vehicular exhaust derived nanoparticles and historical Belgium fortress building interfaces. *Geoscience Frontiers*, *11*(6), 2053–2060. https://doi.org/10.1016/j.gsf.2020.07.003

Taylor, S. R., & McLennan, S. M. (1985). *The continental crust: Its composition and evolution*. Blackwell Scientific Publications . https://www.osti.gov/biblio/6582885

Teran, K., Žibret, G., & Fanetti, M. (2020). Impact of urbanization and steel mill emissions on elemental composition of street dust and corresponding particle characterization. *Journal of Hazardous Materials*, *384*, 120963. https://doi.org/10.1016/J.JHAZMAT.2019.120963

Torres-Sánchez, D., Verma, S. K., Barry, T. L., Verma, S. P., & Torres-Hernández, J. R. (2020). 40Ar/39Ar geochronology and petrogenesis of the Sierra de San Miguelito Volcanic Complex, Mesa Central, Mexico. *Lithos*, *370–371*, 105613. https://doi.org/https://doi.org/10.1016/j.lithos.2020.105613

Torres-Sánchez, D., Verma, S. K., Verma, S. P., Velasco-Tapia, F., & Torres-Hernández, J. R. (2019). Petrogenetic and tectonic implications of Oligocene−Miocene volcanic rocks from the Sierra de San Miguelito complex, central Mexico. *Journal of South American Earth Sciences*, *95*, 102311-. https://doi.org/10.1016/j.jsames.2019.102311

Trechera, P., Moreno, T., Córdoba, P., Moreno, N., Zhuang, X., Li, B., Li, J., Shangguan, Y., Kandler, K., Dominguez, A. O., Kelly, F., & Querol, X. (2020). Mineralogy, geochemistry and toxicity of size-segregated respirable deposited dust in underground coal mines. *Journal of Hazardous Materials*, *399*, 122935. https://doi.org/10.1016/j.jhazmat.2020.122935

UN. (2019). World urbanization prospects 2018: Highlights (ST/ESA/SER.A/421). In *United Nations*. Department of Economic and Social Affairs, Population Division. New York. https://population.un.org/wup/Publications/Files/WUP2018-Highlights.pdf

USEPA. (2007). Method 6200: Field portable X-ray fluorescence spectrometry for the determination of elemental concentrations in soil and sediment. In *Test Methods For Evaluating Solid Waste, US Environmental Protection Agency, Washington, DC, USA*.

https://www.epa.gov/hw-sw846/sw-846-test-method-6200-field-portable-x-ray-fluorescence-spectrometry-determination

Van den Boogaart, K. G., Tolosana-Delgado, R., & Bren, M. (2022). *compositions: Compositional Data Analysis* (2.0-4). https://CRAN.R-project.org/package=compositions

Wei, G., Zhang, C., Li, Q., Wang, H., Wang, R., Zhang, Y., & Yuan, Y. (2023). Characterization of geochemical elements in surface sediments from Chinese deserts. *CATENA*, *220*, 106637. https://doi.org/https://doi.org/10.1016/j.catena.2022.106637

Wheeler, S., Henry, T., Murray, J., McDermott, F., & Morrison, L. (2021). Utilising CoDA methods for the spatio-temporal geochemical characterisation of groundwater; a case study from Lisheen Mine, south central Ireland. *Applied Geochemistry*, *127*, 104912. https://doi.org/https://doi.org/10.1016/j.apgeochem.2021.104912

Wilcox, R. (2011). *Introduction to robust estimation and hypothesis testing* (3rd ed., Vol. 93). Elsevier Science. https://doi.org/10.1016/C2010-0-67044-1

Zeng, J., Luo, X., Cheng, Y., Ke, W., Hartley, W., Li, C., Jiang, J., Zhu, F., & Xue, S. (2022). Spatial distribution of toxic metal(loid)s at an abandoned zinc smelting site, Southern China. *Journal of Hazardous Materials*, *425*, 127970. https://doi.org/10.1016/J.JHAZMAT.2021.127970

Zheng, N., Liu, J., Wang, Q., & Liang, Z. (2010). Health risk assessment of heavy metal exposure to street dust in the zinc smelting district, Northeast of China. *Science of The Total Environment*, *408*(4), 726–733. https://doi.org/10.1016/J.SCITOTENV.2009.10.075

Zoller, W. H., Gladney, E. S., & Duce, R. A. (1974). Atmospheric concentrations and sources of trace metals at the South Pole. *Science*, *183*(4121), 198–200. https://doi.org/10.1126/science.183.4121.198